Supplementary information

Self-damping photonic crystals with differentiated reversible crosslinking domains for biomimetic delayed visual perception of underwater impact stress

Yong Qi[a,b], Jiahui Wang[a], Tong Hu[a], Xianfei Cao[a], Shi Li[a], Qingyu Liu[a], Zhaoyong Gao[a], and Shufen Zhang[a,*]

[a] *State Key Laboratory of Fine Chemicals, Frontier Science Center for Smart Materials, Dalian University of Technology (DUT), Dalian 116024, China*

[b] *Center for Intelligent Biomedical Materials and Devices (IBMD), Shenzhen Institute of Advanced Technology (SIAT), Chinese Academy of Sciences (CAS), Shenzhen 518055, China*

* Corresponding author.

E-mail addresses: zhangshf@dlut.edu.cn

Experimental Section

Materials. DL-thioctic acid (TA) and polyethylene glycol (600) diacrylate (PEGDA) were purchased from Aladdin. 2-hydroxy-2-methyl-1-phenyl-1-propanone (1173, BASF), Hydrofluoric acid (HF, 40 wt %, Fuyu Chemical Reagent Factory), Ammonia solution (25~28 wt %, Tianjin Damao Chemical Reagent Factory), Absolute ethanol (Sinopharm Group Chemical reagent Co., LTD), Tetraethyl orthosilicate (TEOS, SiO_2 > 28 wt %, Xilong Scientific Reagent Factory), Methoxyethyl Acrylate (MEA, Aladdin), Sodium hydroxide (NaOH, Tianjin Tianda Chemical Reagent Factory), Concentrated hydrochloric acid (~36%, Tianjin Damao Chemical Reagent Factory), and Ethyl acetate (Tianjin jingdongtianzheng Precision Chemical Reagent Factory) were used as received.

Fabrication of monodisperse SiO_2 microsphere solution. SiO_2 nanospheres with different particle sizes were prepared under a modified *Stöber* method[1] (so-called seed method). 160 mL ethanol was added to a 250 mL flask, 33 mL deionized water and 3.3 mL ammonia solution were mixed and ultrasonically dispersed for 2 min, and then added to the flask. The mixing system was stirred (speed, 200 r/min) at 60 °C. When the temperature of the mixture rose to 60 °C, 4.4 mL TEOS was added within 10 min. The mixture was stirred for 10 h to obtain a light blue transparent SiO_2 seed solution. 160 mL ethanol, 45 mL deionized water, and 45 mL ammonia solution were added into a 500 mL flask, stirring at room temperature (speed, 300 r/min). 3.3~0.8 mL of the above seed solution was added. The injection pump was used to add 20 mL TEOS (pump speed 0.2 mL/min, a total of 100 min), and then stirred for 5 h. The white solid was obtained by centrifugal separation, and the SiO_2 microspheres were obtained after ultrasonic cleaning with ethanol ("centrifugal-ultrasonic cleaning" three times). Finally, it was dispersed in 60 mL of anhydrous ethanol to obtain a monodisperse SiO_2 microsphere solution (~8 wt %).

Fabrication of SDPCs. SiO_2 opal templates were prepared by using the dip-coating method (pull speed, 2 μm/s, 25 °C). The monodisperse SiO_2 nanosphere solutions (~8 wt %) were prepared by ultrasonic treatment with ethanol. Combining SiO_2 opal templates with glass to form a "sandwich" model, where the gaps between template and glass were separated by polyimide tape (thickness, ~0.3 mm). By utilizing capillary force, the interstitials in between SiO_2 nanospheres of the "sandwich" model were filled up with monomer mixtures consisting of TA and PEGDA with a mass ratio of 900:900 (mg/mg). Darocur 1173 (1 μL) could be added as the photoinitiator. The monomer-filled "sandwich" model was photopolymerized by using a

pulsed UV curing system (UVGO UV Curing Lamp, 100 W) for 15 min. The composite film was peeled off after soaking in hot water for 1 h. The composite film was soaked in a 5-volt % HF aqueous solution for 5 min and finally rinsed with water and absolute ethanol. The obtained SDPCs were stored in water for further use.

Degradation experiment. The 0.1 g SDPC was ground into powder, and then added to a 10 mL NaOH solution (5 mg/mL), stirring at room temperature to dissolve. The solution changed from light yellow to orange with the extension of stirring time. The pH was adjusted to ~5 with dilute hydrochloric acid, and 5 mL ethyl acetate was added for extraction. The organic phase was concentrated to form a yellow solid or oil.

Fe^{3+}-induced coordination: SDPC was cleaned with anhydrous ethanol and placed in a $FeCl_3$ ethanol solution (0.1 g/mL) at room temperature. The stiffness of SDPC increases with time.

Indentation test. The samples were immersed in water. The typical indentation force-displacement curve of the water-wetted SDPC was recorded by a Micromechanical Testing and Assembly System (FT-MTA03). The maximum depth (start by reaching the max trigger contact force) is 5 μm. The max trigger contact force during approaching is 50 μN. The approaching and retracting speed is 0.5 μm/s, and the hold time is 0 s. For the isobaric relaxation curve of water-wetted SDPC during indentation, at the max compression depth (5 μm, start by reaching the max trigger contact force), the probe was suddenly withdrawn to a force of 0.1 mN, automatically maintaining the contact force and recording the change of displacement with time. The hold time is 600 s.

2D correlation analysis of FTIR spectra. The time-dependent in-situ FTIR spectra during rebound were recorded by a Fourier Transform Infrared Spectrometer (Thermo Fisher iS50, United States). Test mode: Reflection. The water-wetted SDPC was sealed at the probe. The film was compressed through an indenter. The initial spectrum was scanned and recorded at compressed states. After relaxing, the spectra during the rebounding were recorded every 15 s. The recorded FTIR spectra were further used to perform corresponding 2D correlational analysis on the software 2D Shige ver. 1.3 (Shigeaki Morita, Kwansei-Gakuin University, Japan, 2004-2005). 2D correlation analysis of FTIR spectra can distinguish the priority of the characteristic groups during the response of the material, which is particularly useful for

corresponding analysis at the molecular engineering level.[2] A summary of Noda's rule can be found in the above literature.

Characterizations. The scanning electron microscope (SEM, Nova Nano SEM 450; Testing Conditions: HV, 10 kV; Spot, 3.0) was used to characterize the corresponding morphology of the SDPCs. An atomic force microscope (AFM, Dimension ICON) was used to scan the surface morphology and corresponding phase images of SDPCs. The reflectance spectra of the SDPCs under different testing conditions were recorded by a Fiber Optic Spectrometer (EQ 2000). Huawei Honors V20 was used to capture all the photos of the SDPCs. The tensile strength and adhesion tests were conducted with the PT-305 Computer universe testing machine from Dongguan Precise-test Equipment Co., Ltd. The ultra-depth-of-field microscope (VHX-7000, Keyence) was used to observe the in-situ structural deformation of water-wetted SDPC during rebound. The indentation force-displacement curves and isobaric relaxation curves of water-wetted SDPCs were recorded by a Micromechanical Testing and Assembly System (FT-MTA03, Switzerland). FTIR spectra of SDPCs during photopolymerization were collected by an Advanced Fourier Transform Infrared Spectrometer (Thermo Fisher 6700, KBr pellet). In-situ FTIR spectra of SDPCs during rebound were collected by a Fourier Transform Infrared Spectrometer (Thermo Fisher iS50, United States). The Raman spectra of SDPCs during photopolymerization were recorded by a Laser confocal microraman spectroscopy (Renishaw, inVia Qontor, 785 nm). The ^{1}H NMR spectra of the degradation product were characterized by a nuclear magnetic resonance (NMR) spectrometer (Bruker AVANCE III 500, Bruker, Switzerland). A freeze-dried SDPC sample was obtained by using a freeze dryer (Beijing Boyikang Experimental Instrument Co., ltd). The molecular weight was determined by gel permeation chromatography (GPC) on an Agilent 1200 instrument with water as the mobile phase. ESCALABTM 250Xi from Thermo Fisher was used for X-ray photoelectron spectroscopy (XPS).

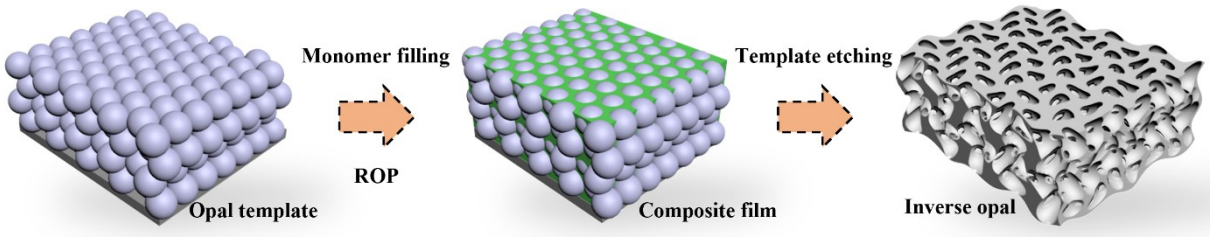

Fig. S1. SDPC prepared by template negative copy method.

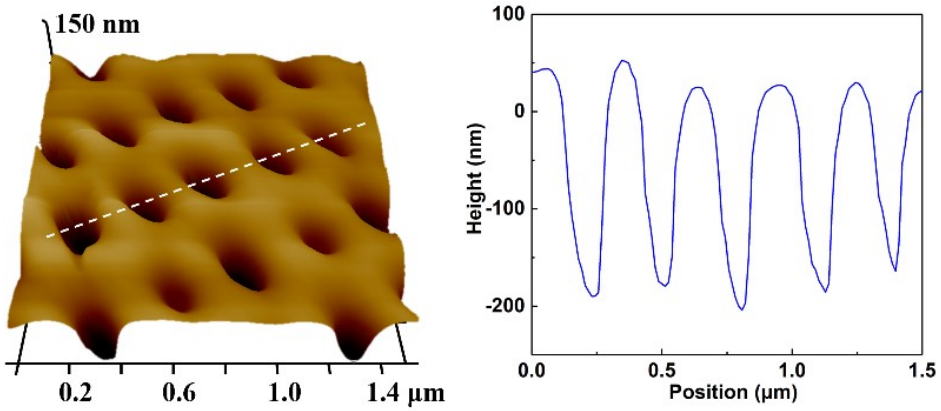

Fig. S2. Atomic force microscope image and the height profile scanned across the profile line of SDPC in water. The SDPC displays a 3D-ordered inverse opal structure in water.

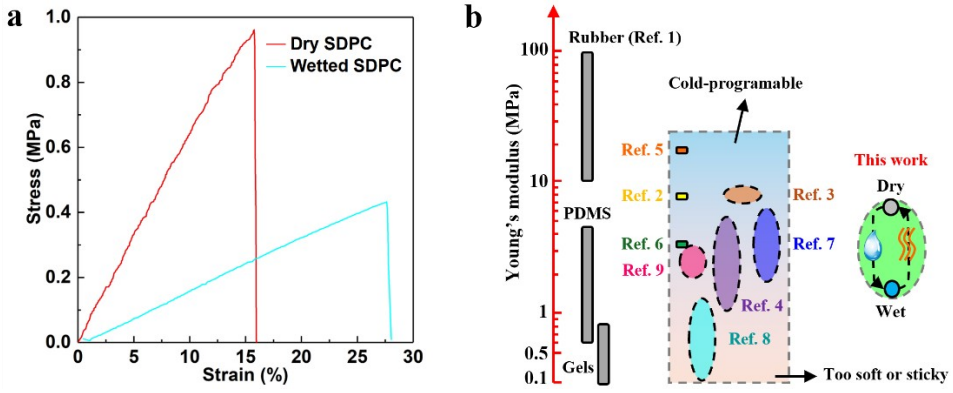

Fig. S3. a) Stress-strain curves of the dry and water-wetted SDPCs; b) Young's modulus (*E*) of the dry and water-wetted SDPCs. Diagram of the dry-wet *E* conversion of SDPC and the *E* of reported deformable macropores.[3-11]

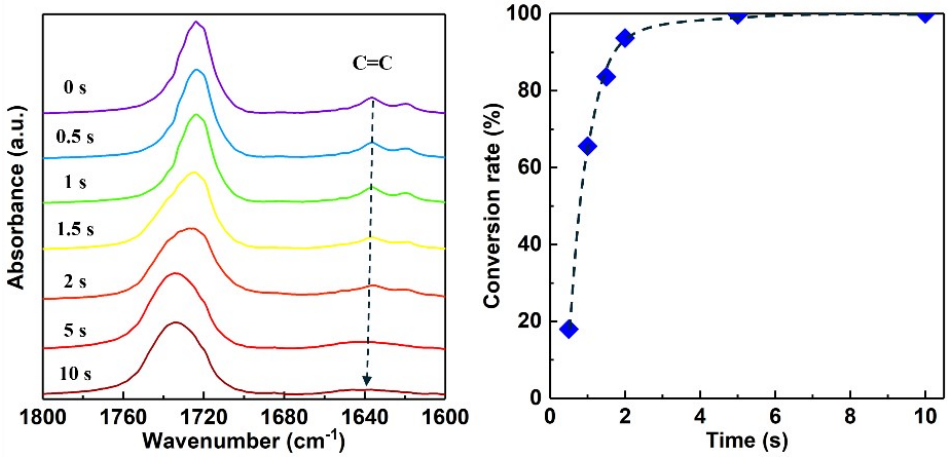

Fig. S4. The time-dependent FTIR spectra of the PEGDA-600 during photopolymerization (monomer, 1800 mg; photoinitiator 1173, 1 μL) in the regions of *ν*(C=O) and *ν*(C=C). On the right is the corresponding time-dependent conversion rate of C=C. PEGDA-600 can be completely polymerized within 10 s, while the photopolymerization time of TA and PEGDA blend system takes 15 min (**Fig. 1e**), which fully demonstrates the strong inhibition effect of TA on PEGDA-600 photopolymerization activity.

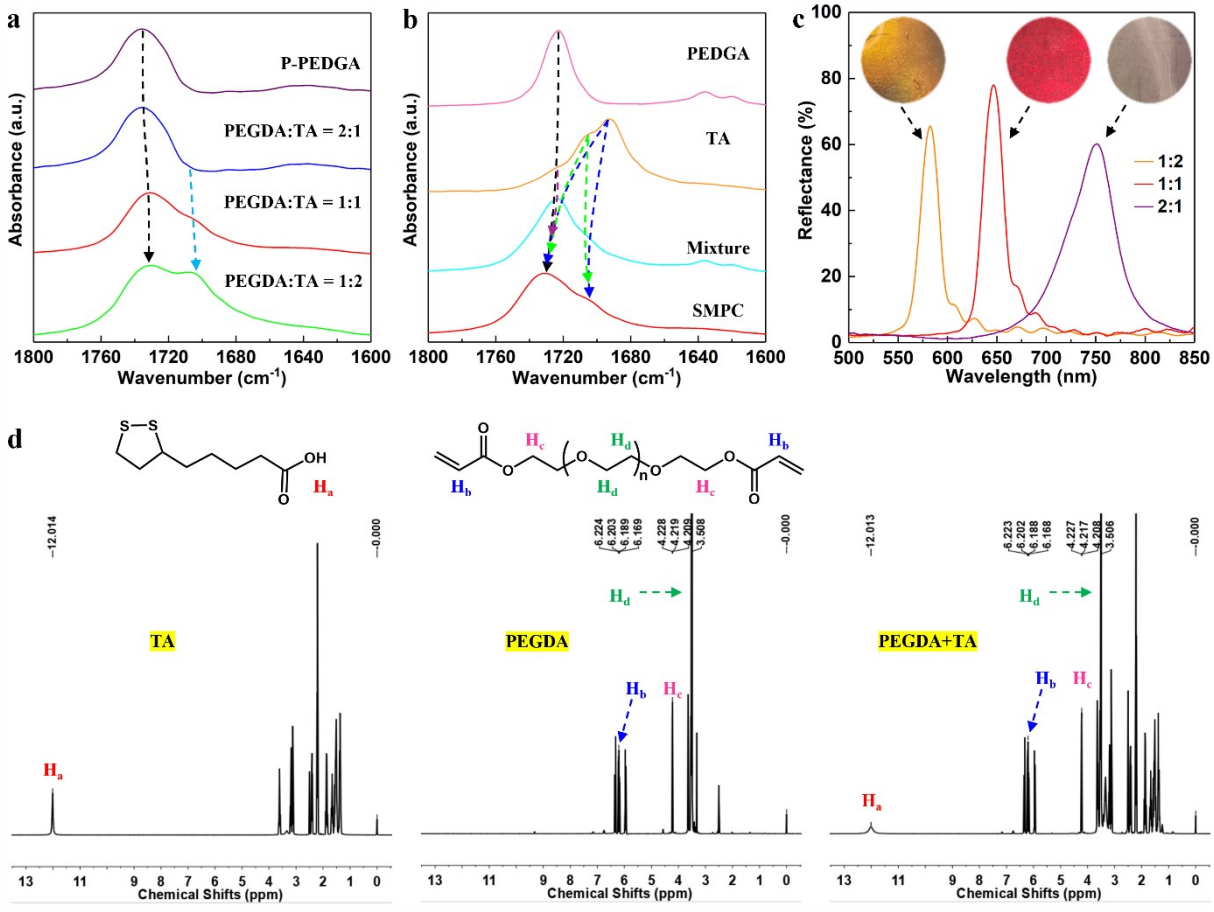

Fig. S5. Screening of monomer ratio for preparing SDPC. a) The FTIR spectra of the prepared PCs with different monomer ratios in the region of *ν*(C=O); b) The FTIR spectra of the

monomers, mixture, and prepared SDPC in the region of ν(C=O); c) Reflection spectra of prepared PCs with different monomer ratio in water. The insets are corresponding photos; d) ^{1}H NMR (Dimethylsulfoxide-*d*6, DMSO-*d*6) spectra of TA, PEGDA, and their mixtures (mass ratio, 1:1). Typical H, which might be affected by the interaction between the neighboring group and H-bond, is highlighted.

Before polymerization, the chemical shift of H near the ester group and ether in the mixed monomer moves to the higher field, and the signal of COO**H** (H_a) becomes wider and the intensity decreases, which fully indicates the weak interaction between TA and PEGDA. With the increase of TA, after polymerization, the content of dimer COOH (~1705 cm^{-1}) increased, and the absorption peak of C=O moved to a lower wavenumber (from ~1736 to ~1731 cm^{-1}), indicating that the distribution density of weak and strong H-bonds increased. In pure TA, COOH produced three distinct absorption peaks of ~1725, ~1705, and ~1693 cm^{-1}. This might be attributed to the different aggregation states of COOH, even producing H-bond clusters. For PEGDA:TA=1:1, the main absorption peak (~1723 cm^{-1}) of the monomer mixture was biased towards PEGDA, indicating that the COOH of TA interacted with PEGDA, and the density of the dimer COOH decreased. After polymerization, the main peak of C=O shifted towards a higher wavenumber (from ~1723 to ~1731 cm^{-1}), which can be attributed to the dispersion of TA by the PEGDA chain (possibly increasing free COOH, ~1758 cm^{-1}). In addition, the absorption strength of dimer COOH increased at ~1705 cm^{-1}, indicating that the polymerization enhanced and consolidated the strong H-bond clusters. The increase of the FWHM of the absorption peak of C=O could be attributed to the strengthening of the weak H-bonds. The PCs prepared with the three ratios showed different reflection and structural colors in water. Among them, PEGDA:TA=2:1 shows strong hydrophilicity and swelling, and the corresponding λ_{max} is close to the near-infrared region (~750 nm). PEGDA:TA=1:2 displays anti-swelling properties (which can be attributed to the self-sealing of the dimeric COOH,[12-14] inhibiting the binding of water to the chain), corresponding to a λ_{max} of ~580 nm. PEGDA:TA=1:1 corresponds to the λ_{max} of ~650 nm, which is suitable for the study of elastic deformation and rebound of macropores (a larger visible region of structural color change during compression or rebound). The weak/strong H-bond in SDPC will play a buffer role during the elastic deformation and rebound of macropores.[15, 16]

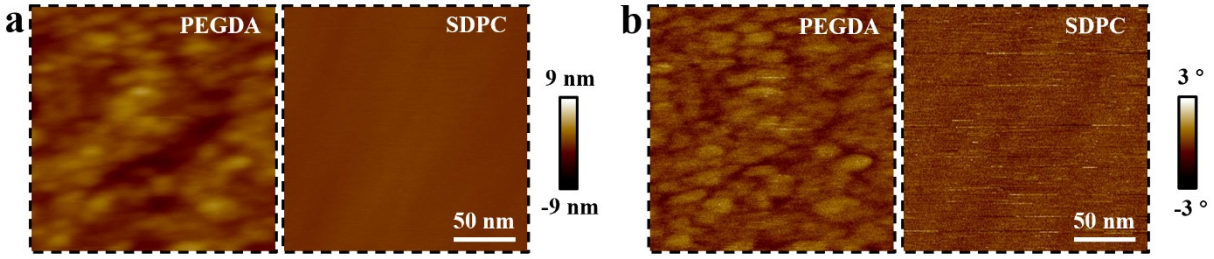

Fig. S6. (a) AFM height images and (b) corresponding phase images of the polymerized PEGDA film and SDPC.

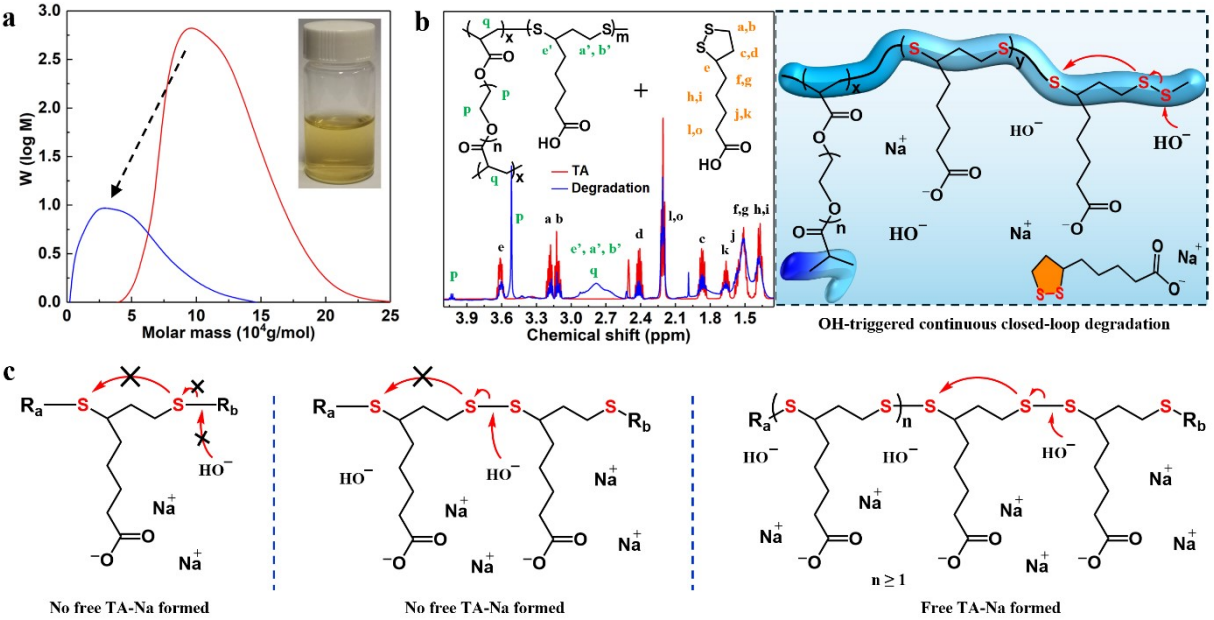

Fig. S7. Closed-loop degradation experiment. a) The typical GPC of the reaction solution during SDPC degradation. The inset shows the typical photo of the reaction solution; b) The ^{1}H NMR (Dimethylsulfoxide-*d*6, DMSO-*d*6) spectra of the TA and degradation product. The diagram on the right shows the relevant closed-loop degradation mechanisms; c) Possible copolymerization derived from the closed-loop degradation of TA.

As the time went by, the average molecular weight decreased from ~100000 to ~30000 g/mol. This means that the degradation reaction constantly releases small molecular compounds. The complete dissolution of the polymer powder indirectly also proves that PEGDA copolymerizes with TA, which would otherwise produce insoluble products. The ^{1}H NMR spectroscopy shows that the chemical shift at 2.50~3.00 ppm could be attributed to the oligomer of PEGDA-*co*-TA. The chemical shift at ~4.03 and ~3.51 ppm belongs to -O-C**H**$_2$-C**H**$_2$-O- of the PEGDA chain segments. FTIR and Raman spectra showed that PEGDA and TA were basically copolymerized (**Fig. 1e**). Compared with the ^{1}H NMR of pure TA, free TA exists

in the degradation products, which can only be derived from the closed-loop depolymerization of SDPC. According to the closed-loop degradation mechanism of polymerized TA in NaOH solution reported in the literature,[17] the OH^- attacks the S-S bond to produce sulfur anion. The sulfur anion then attacks the adjacent S-S bond, forming free TA and a new sulfur anion. When there is no S-S bond nearby, the continuous closed-loop degradation reaction will be terminated. Therefore, the necessary condition for the formation of free TA is the presence of at least three continuous TA units in the middle of the polymer chain or two continuous TA units at the end of the chain. Our degradation experiments fully demonstrated that the differentiated polymerization of PEGDA and TA resulted in the aggregation of TA units. According to the degree of aggregation, COOH with high aggregation produces strong H-bond clusters, while TA with partial random copolymerization can only form weak H-bonds with neighboring groups (such as ester groups and ethers) due to chain tension.[18] The aggregation of weak H-bonds forms weak H-bond clusters.

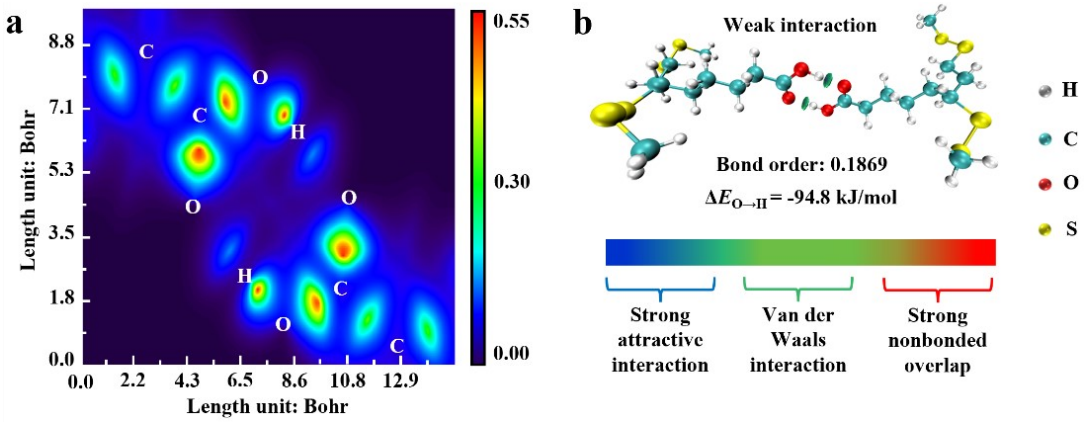

Fig. S8. Density functional theory (DFT) based molecular designing.[19, 20] (a) The plane map of the difference of gradient of promolecular density (δg) based on DFT. Warm colors represent high ED distribution. The atoms are replaced with their element symbols; (b) Possible structures of the single fragments of dimer and color-filled independent gradient model based on Hirshfeld partition of molecular density (IGMH) plot, showing the interaction of strong H-bond. The corresponding Mayer bond order was calculated based on DFT, which is a physical quantity describing the bond strength between adjacent atoms in the molecule and represents the relative strength of the bond.

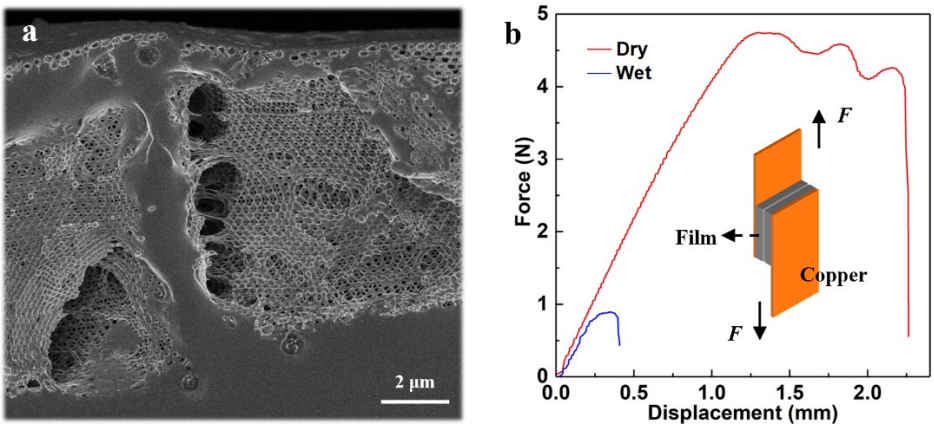

Fig. S9. (a) Typical cross-sectional SEM images of freeze-dried SDPC; (b) Adhesion test of SDPC in the dry and water-wetted state. SDPC (1 cm^2) was pasted onto two copper sheets, pressure was applied to force the two SDPCs to adhere, and the change in the relevant tension was recorded by a tensile tester. The adhesion force of SDPC decreased by ~8 times after water wetting.

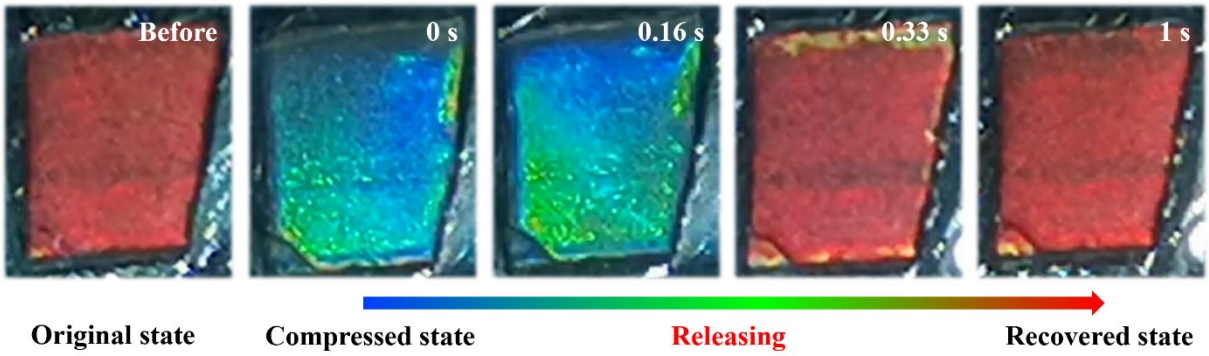

Fig. S10. Real-time structural color imaging of control PC sample (TA was replaced by MEA, and the monomer ratio was the same as SDPC) during rebounding in water.

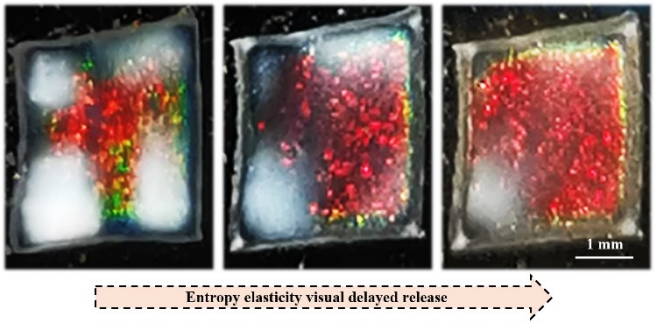

Fig. S11. Photos of a typical SDPC during rebound under a dual-light source. The natural light source is located directly above the film, the polarized light source is located directly below the film, and the polarizer is located between the natural light source and the film. The stress concentration of SDPC appears white under polarized light. With the increase of rebound time, SDPC gradually returns to red, and the white area gradually decreases and fades.

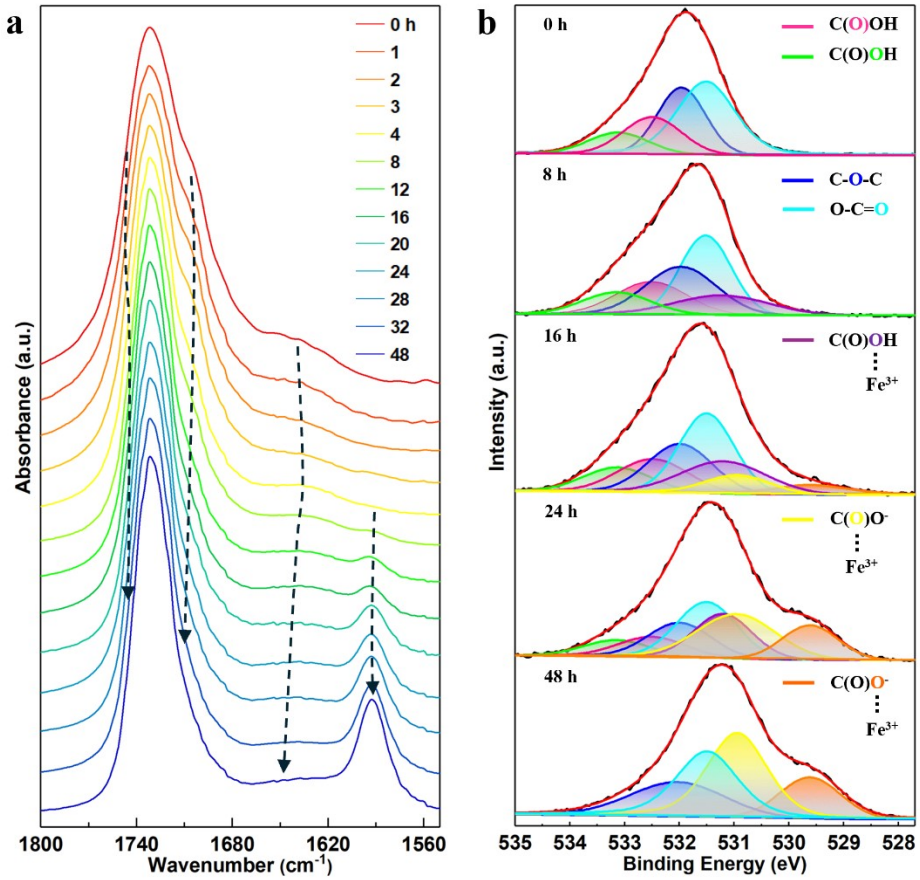

Fig. S12. The destroying of the weak and strong crosslinking domains by Fe^{3+}-crosslinking. (a) The time-dependent FTIR spectra of the SDPC during Fe^{3+}-coordinating in the regions of *ν*(C=O); (b) XPS spectra of O1s of the SDPCs with different Fe^{3+}-coordinating times.

FTIR and XPS spectra showed that COOH (especially the dimer) first weakly interacts with Fe^{3+} (ν(C=O) fluctuates at ~1638 cm^{-1} and O1s produces a new peak at ~531.21 eV), invading the weak/moderate crosslinking domains as the coordination time increases. Then the dimeric COOH was opened by electron-deficient Fe^{3+}, which was confirmed by the weakening of ν(C=O) at ~1705 cm^{-1} and the fracture strain (first increase and then decrease). The fact that the opening of the domains takes a long time also indirectly explains the existence of H-bond clusters. After 8 h, the characteristic absorption peak of the typical carboxylate (ν(C=O), ~1592 cm^{-1}; O1s, ~530.94 and ~529.62 eV) gradually enhanced, which can be attributed to the deprotonation and Fe^{3+}-O formation. Subsequently, the Fe^{3+}-coordinated trimers gradually increased to form stronger crosslinking sites.[21] The sharp decrease of the FWHM of the main ν(C=O) at ~1730 cm^{-1} indicates the disappearance of H-bond clusters.

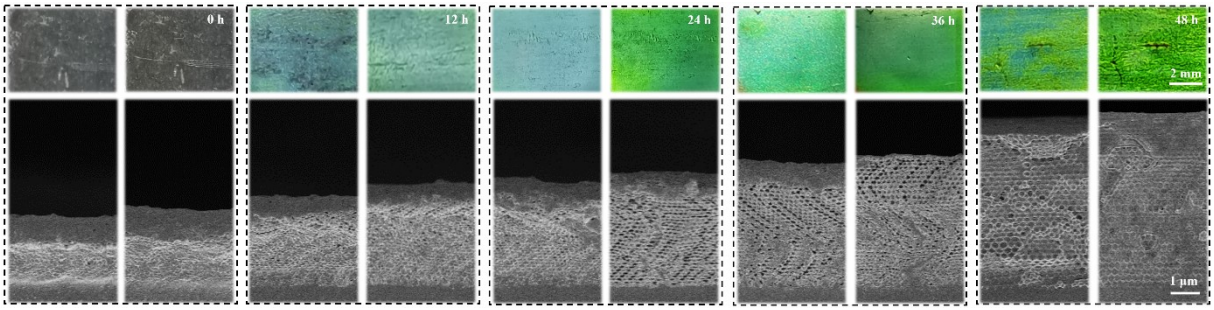

Fig. S13. Corresponding photos and typical cross-sectional SEM images of SDPCs with different Fe^{3+}-coordinating times. The left side corresponds to the sample after water evaporation, and the right side corresponds to the sample after ethanol evaporation.

With the increase of Fe^{3+}-coordinating time, the reflection of SDPCs after solvent evaporation gradually enhanced and redshifted, and the structural color changed from colorless to green. SEM recorded the orderly recovery of the inverse opals. We suspect that Fe^{3+}-coordination disrupts the weak/strong crosslinking domains while simultaneously converging the crosslinking sites, increasing the strength of SDPC. Fe^{3+} breaks the binding balance of weak/strong crosslinking domains to the polymer network through diffusion and coordination, increasing the crosslinking density and decreasing the H-bond-induced adhesion.

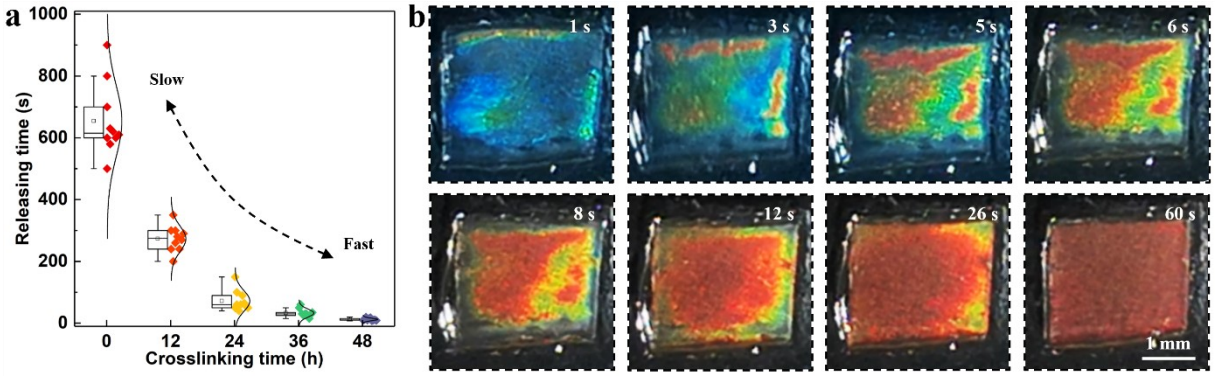

Fig. S14. (a) Statistics of the release time of entropic elasticity of the SDPC with different Fe^{3+}-coordinating time; (b) Real-time structural color imaging of "SDPC-Fe^{3+}-24h" during the typical entropic elasticity release.

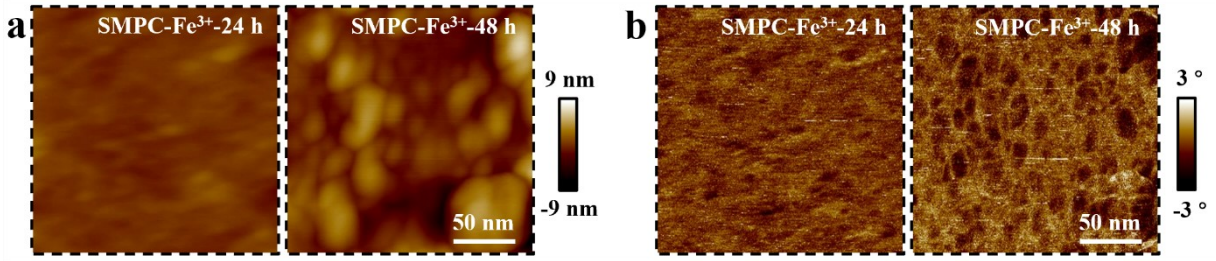

Fig. S15. (a) AFM height images and (b) corresponding phase images of the "SDPC-Fe^{3+}-24h" (SDPC coordinating with Fe^{3+} for 24h) and "SDPC-Fe^{3+}-48h" (SDPC coordinating with Fe^{3+} for 48h).

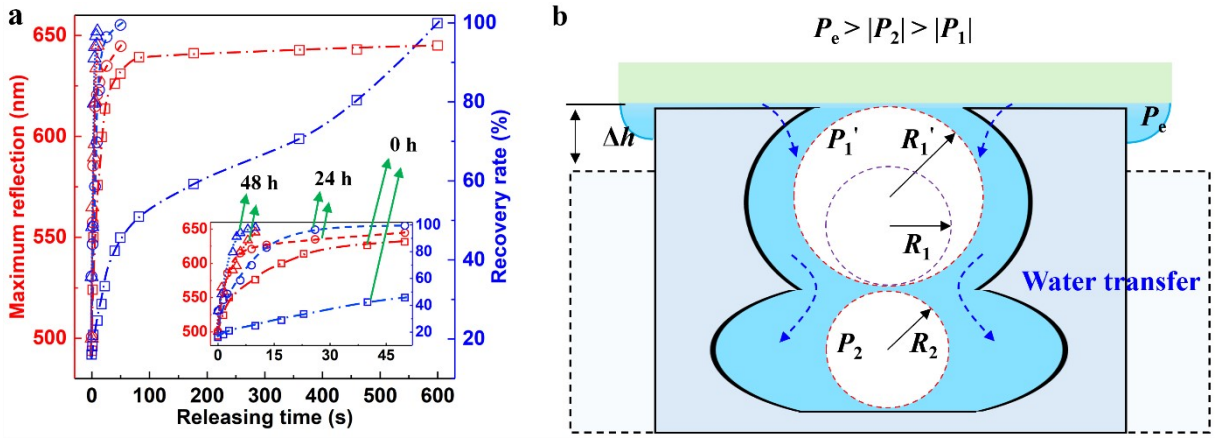

Fig. S16. (a) The λ_{max} and the corresponding η (recovery rate, the ratio of the maximum reflection intensity at time t to that before compression) during the typical rebounding of water-wetted SDPCs after Fe^{3+}-coordinating for 0 h (box), 24 h (circle), and 48 h (triangle); (b)

Schematic diagram of a typical asymmetric transformation during the macropore rebound at the nanostructure engineering level.

For the capillary pressure,[4, 6] $P = (2\gamma \cos \theta)/R$, at the initial stage of release, it is estimated that the P generated in the internal and external macropores is the same (P_1=P_2, R_1=R_2), that is, there is:

$$P_1 = \frac{2\gamma\cos\theta}{R_1} \tag{1}$$

$$P_2 = \frac{2\gamma\cos\theta}{R_2} \tag{2}$$

The instantaneous recovery thickness (Δh, change in thickness at some point in time) of SDPC can be expressed by the recovery rate (η):

$$\Delta h = 2R_1\eta \tag{3}$$

$$R_1' = (1+\eta)R_1 \tag{4}$$

The corresponding transient Laplacian pressure difference can be expressed as:

$$\Delta P = 2\gamma\cos\theta\left(\frac{1}{R_1'} - \frac{1}{R_2}\right) \tag{5}$$

$|\Delta P|$ could be simplified as:

$$\frac{1}{R_1'} - \frac{1}{R_2} = \frac{1 \quad -\eta}{R_1 1+\eta} \tag{6}$$

$$|\Delta P| = |P_1|\frac{\eta}{1+\eta} \tag{7}$$

For SDPC and Fe^{3+}-coordinated SDPCs, the derived $|\Delta P|$ is an increasing function of the η. P_1 is the initial capillary pressure of the macropore during rebound. At the same time node, Fe^{3+}-coordinated SDPC shows a larger η (**Fig. S16a**). Therefore, a larger $|\Delta P|$ will be obtained, accelerating the solvent transfer in asymmetric macropores and shortening the associated equilibrium time.

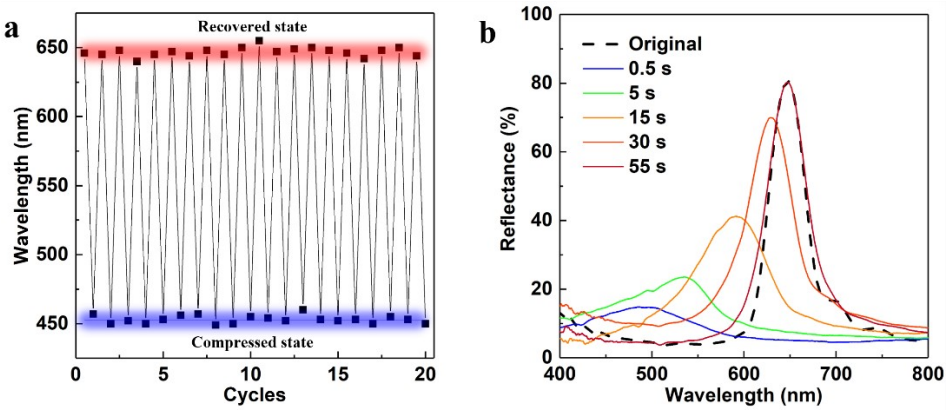

Fig. S17. (a) Cycles of the SDPC during compression-rebound; (b) The reflection spectra of SDPC after withdrawing the indenter. The pressure is ~25 N.

Video 1. Real-time structural color imaging of water-wetted SDPC during the typical entropic elasticity delayed release. (incident angle, 0°; detection angle, 0°).

Video 2. Real-time structural color imaging of water-wetted control PC sample (TA was replaced by methoxyethyl acrylate, and the monomer ratio was the same as SDPC) during the typical entropic elasticity delayed release. (incident angle, 0°; detection angle, 0°).

Video 3. Real-time polarized optical imaging of water-wetted SDPC during the typical entropic elasticity delayed release.

Video 4. Typical time-dependent evolution of the structural color pattern, the stamp was immediately withdrawn after imprinting on the SDPC (underwater, incident angle, 0°; detection angle, 0°).

Video 5. Alternate editing of structural color patterns on SDPC (underwater, incident angle, 0°; detection angle, 0°).

Video 6. Typical time-dependent evolution of the structural color pattern, the stamp was immediately withdrawn after imprinting on the "SDPC-Fe^{3+}-48h" (underwater, incident angle, 0°; detection angle, 0°).

References

1 W. Stöber, A. Fink and E. Bohn, *J. Colloid Interface Sci.* 1968, **26**, 62-69.

2 J. Wu, B. Wu, J. Xiong, S. Sun and P. Wu, *Angew. Chem. Int. Ed.*, 2022, **61**, e202204960.

3 S. Li, B. Deng, A. Grinthal, A. Schneider-Yamamura, J. Kang, R.S. Martens, C.T. Zhang, J. Li, S. Yu, K. Bertoldi and J. Aizenberg, *Nature*, 2021, **592**, 386-391.

4 Y. Fang, Y. Ni, S.Y. Leo, C. Taylor, V. Basile and P. Jiang, *Nat. Commun.*, 2015, **6**, 7416.

5 Y. Qi, L. Song, C. Zhou and S. Zhang, *Adv. Mater.*, 2023, **35**, 2210753.

6 S.-Y. Leo, Y. Ni, C. Xu, Y. Zhang, Y. Dai, P. Qi, A.T. Xie, V. Basile, C. Taylor and P. Jiang, *Adv. Funct. Mater.*, 2017, **27**, 1703522.

7 Y. Fang, Y. Ni, B. Choi, S.Y. Leo, J. Gao, B. Ge, C. Taylor, V. Basile and P. Jiang, *Adv. Mater.*, 2015, **27**, 3696-3704.

8 X. Chen, G. Han, P. Ren, Q. Lyu, M. Li, L. Zhang and J. Zhu, *Chem. Eng. J.*, 2022, **446**, 136879.

9 Y. Qi, D. Kou, Y. Sun, T. Hu, H. Yuan, C. Zhou, C. Li, A.-H. Lu, S. Wu and S. Zhang, *Chem. Eng. J.*, 2023, **457**, 141184.

10 Z. Wang, F. Meng, M. Kong, X. Guo, S. Zhang, Y. Zhang and B. Tang, *Small*, 2023, **20**, 2305825.

11 Z. Wang, S. Zhang and B. Tang, *ACS Nano*, 2023, **18**, 186-198.

12 Y. Qi, W. Niu, S. Zhang, S. Wu, L. Chu, W. Ma and B. Tang, *Adv. Funct. Mater.*, 2019, **29**, 1906799.

13 Z.S. Nurkeeva, G.A. Mun and V.V. Khutoryanskiy, *Macromol. Biosci.*, 2003, **3**, 283-295.

14 J. Wang, J. Hu, Y. Wen, Y. Song, and L. Jiang, *Chem. Mater.*, 2006, **18**, 4984-4986.

15 Y. Cheng, Y. Zhou, R. Wang, K.H. Chan, Y. Liu, T. Ding, X.Q. Wang, T. Li and G.W. Ho, *ACS Nano*, 2022, **16**, 18608-18620.

16 Q. Zhang, C.-Y. Shi, D.-H. Qu, Y.-T. Long, B. L. Feringa and H. Tian, *Sci. Adv.*, 2018, **4**, eaat8192.

17 Q. Zhang, Y. Deng, C.-Y. Shi, B.L. Feringa, H. Tian and D.-H. Qu, *Matter*, 2021, **4**, 1352-1364.

18 W. Zhao, B. Wu, Z. Lei and P. Wu, *Angew. Chem. Int. Ed.*, 2024, **63**, e202400531.

19 T. Lu and Q. Chen, *J. Comput. Chem.*, 2022, **43**, 539-555.

20 T. Lu and F. Chen, *J. Phys. Chem. A*, 2013, **117**, 3100-3108.

21 Q. Zhang, D.H. Qu, B.L. Feringa and H. Tian, *J. Am. Chem. Soc.*, 2022, **144**, 2022-2033.